Short Communication

Synthesis and characterization of transition metals doped CuO nanostructure and their application in hybrid bulk heterojunction solar cells

Muzaffar Iqbal[1,2] · Akbar Ali[1,2] · Khuram Shahzad Ahmad[3] · Farhat Mehmood Rana[4] · Jamshid Khan[5] · Karim Khan[6] · Khalid Hussain Thebo[2,7]

Abstract

Herein, transition metals i.e. Mn, Fe doped CuO nanostructures were synthesized via simple and facile wet chemical method. As-prepared materials were characterized by X-ray diffraction (XRD), scanning electron microscope (SEM), energy dispersive X-ray spectroscopy (EDX), transmission electron microscope (TEM), ultraviolet–visible and emission spectroscopy. The XRD studies reveal that doped and un-doped CuO have single phase, suggesting the incorporation of Mn and Fe dopants in CuO lattice. Further, as-synthesized materials were used in the hybrid bulk heterojunction organic solar cell and it was found that the low concentration of doping increase the charge separation led to enhance the power conversion efficiency of the device as compared to high amount of doping. This increase in the power conversion efficiency of the prepared devices is mostly due to increase in fill factor and short-circuit current density upon doping of Mn:Fe to CuO nanostructures.

Keywords CuO · Nanostructures · Hybrid · Heterojunction · Solar cell

1 Introduction

Metal oxide nanostructures such as ZnO, NiO, CuO, TiO_2 etc. with narrow and large band gap based p and n-type, have been widely investigated for their potential applications in various energy and environmental sectors [1–8]. Among these, copper oxide (CuO) has attended significant interest due to its exciting surface chemistry, excellent recyclability, non-toxicity, relatively high abundance, affordable cost and has been widely explored as an innovtaive material for solar cell and photovoltaics (PV) applications [9–13]. In this regard, several efforts have been carried out to use CuO in the PV application in the form of nanorods, nanospheres, nanotubes, nanoribbons, microworms and microflowers. Besides this, numbers of transition metals have been used as dopants to alter the physical and chemical properties of CuO nanostructures. In fact, the transition metal ions dopant create an impurity level between the conduction and valence band which act as an intermediate step to support the electron during excitation upon photon absorption [14–18]. These impurity levels can consider as an acceptor levels, deep recombination centers and shallow donor [19, 20]. Unfortunately, these sufficient deep defect states support recombination center of excitons (e^- and h^+) beside assisting in providing the transition

✉ Khalid Hussain Thebo, Khalidthebo@yahoo.com | [1]National Centre for Nanoscience and Technology, Chinese Academy of Sciences, Zhongguancun, Beijing 100190, People's Republic of China. [2]University of Chinese Academy of Sciences (UCAS), Beijing 100043, People's Republic of China. [3]Department of Environmental Sciences, Fatima Jinnah Women University, The Mall, Rawalpindi 46000, Pakistan. [4]Department of Chemistry, University of Education Lahore, D. G. Khan Campus, Kangan Road, D. G. Khan, Pakistan. [5]Department of Chemistry, Hazara University Mansehra, Mansehra, Khyber Pakhtunkhwa 21300, Pakistan. [6]College of Electronic Science and Technology, THz Technical Research Center of Shenzhen University, Shenzhen 518060, People's Republic of China. [7]Dr. M. Kazi Institute of Chemistry, University of Sindh, Jamshoro, Pakistan.

SN Applied Sciences (2019) 1:647 | https://doi.org/10.1007/s42452-019-0663-5

Received: 21 March 2019 / Accepted: 22 May 2019 / Published online: 28 May 2019

states for the excited electrons required lower energy than pristine material and suppressing the recombination by acting as traps when shallow, leading to delay recombination [19–21].

On the other side, mostly research on hybrid (organic–inorganic) solar cells are focused on binary systems, while studies on ternary systems consist of polymers such as phenyl-C_{61}-butyricacid-methyl ester (PCBM) and nanocrystals are rarely reported [22, 23]. Chin et al. [24] enhanced the short circuit current density by integrating gold (Au) nanocrystals in a poly-(3-hexylthiophene) (P3HT):PCBM system. Furthermore, ternary blend devices are very plain and efficient method to further enhance the performance of a device [25, 26]. Short-circuit current density (Jsc) can be easily tuned in these blend system by the conjugation of a light-harvesting donor material to absorb solar spectrum similar to P3HT:PCBM binary blends [27, 28]. In the present era, organic solar cells assembled mostly with the ternary blends of P3HT, silicon phthalocyanine bis(trihexylsilyl oxide) (SiPc) and PCBM, due to SiPc has the absorption band in the near-infrared region, leading to improvement of Jsc [29]. Moreover, hybrid devices based on ternary blends of P3HT:PCBM with NiO, CuO, TiO_2 and ZnO are reported [25, 30–32]. This addition of inorganic semiconductors in the organic blend boosted the Jsc due to absorption of nanoparticles in the UV-region and formed percolation network to facilitate charges in the active layer [30]. Among these, CuO is most desirable and promising materials has higher optical absorption, relatively low cost of raw materials. The band gap is around 1.5 eV, which is very close to the ideal energy gap of 1.4 eV for photovoltaics (PV) devices and considered as a splendid absorber of sunlight [33]. Furthermore, the doping of CuO with different transition metals such as Mn, Fe, Zn etc. [33–35] are also an effective strategy to improve the PCE of the PV devices. The observed improvement is ascribed to the formation of defect states right below the conduction band of Mn [23]. Similarly, Fe doped CuO has been tested to have a productive effect on the solar cell efficiency [36]. From the above studies, it is clear that doping with Mn and Fe should have a synergistic effect on the solar cell efficiency of CuO particularly as the band gap reduction is expected.

In this study, CuO nanostructure with various ratios of Mn and Fe doping were synthesized using simple wet chemical method and were fully characterized. The effect of Mn and Fe doping to CuO were investigated in detail. Further, as-prepared nanostructures were deployed as an electron acceptor material with the fixed amount of conjugated polymer i.e. P3HT blend. We hope this work will provide a new opportunity for scientific community to further investigate the chemistry behind these nanostructure materials to further improve the efficiency of solar cell.

All the chemicals were of analytical grade and used as received. Copper acetate ($Cu(CH_3COO)_2{\cdot}H_2O$, 99.9%), ferric chloride ($FeCl_3$), and manganese dichloride tetrahydrate ($MnCl_2{\cdot}4H_2O$), sodium hydroxide (NaOH), thioglycerol, poly(3,4-ethylene dioxythiophene): polystyrene sulfonate-PEDOT:PSS) (99.5%) and poly(3-hexylthiophene-2,5-diyl-P3HT) (99.9%) were purchased from Alfa Aesar Co., Ltd, China. Milli-Q ultra-pure water with a resistivity higher than 18.2 MΩ cm was used in the experiment.

The CuO nanotubes were prepared by according to modified method [37]. Initially $Cu(CH_3COO)_2{\cdot}H_2O$ (1.0 M) and NaOH (5.0 M) were dissolved in de-ionized (DI) water separately under continuous stirring. Further, 1.0 µL of thioglycerol solution was added dropwise to the $Cu(CH_3COO)_2{\cdot}H_2O$ solution and stirred for 10 min. After that NaOH solution was mixed in above mixture, followed by addition of water under constant stirring. Finally, precipitates were collected, washed with several times with DI water and dried in an oven overnight at 35 °C.

To investigate the effect of doping of Mn and Fe in CuO nanotubes were successfully synthesized. 1.0 M concentration of NaOH with oxygen (O_2) source along $FeCl_3$ (0.4 M) and $MnCl_2{\cdot}4H_2O$ (0.6 M) as a Fe, Mn-dopant precursor. For the Cu source, 1.0 M $Cu(CH_3COO)_2{\cdot}H_2O$ was dissolved in double distilled water for the preparation of all solutions as described earlier. For the synthesis of the un-doped CuO nanotubes equal ratio (1:1) of 1.0 M $Cu(CH_3COO)_2{\cdot}H_2O$, NaOH and thioglycerol (TG) as a capping agent were mixed in a 100 mL flask under constant stirring. In order to prepare different ratios (2, 4 and 6)% of (Mn + Fe) doped CuO nanotubes, an equal amount of different concentrations of the $MnCl_2{\cdot}4H_2O$ and $FeCl_3$ like 0.2, 0.4 and 0.6 M was added to the above mixture dropwise followed by addition of distilled water. As-prepared solutions were stirred for 1 h to collect the doped CuO precipitates. These precipitates were centrifuged, washed several times with distilled water and dried at 40 °C under vacuum oven for 12 h.

The synthesized Mn and Fe doped nanostructures used as photoactive acceptor materials with different ratios (i.e. 2, 4 and 6% prepared in 5.0 mL methanol). On the other side, poly-3-hexyl thiophene (P3HT) (20 mg/mL) was prepared using the same solvent in an inert atmosphere (argon gas) and mixed both solutions properly. A glass sheet substrate of 3×2 cm^2 dimensions covered with transparent conducting oxide ITO (80 nm) and etched desired area with Zn metal doped hydrochloric acid (32%). These glass substrate was washed with ethanol, acetone and distilled water (5 min each) and dried under N_2 stream in order to remove traces of HCl. Initially, a thin layer of PEDOT-PSS-(poly(3,4-ethylene dioxythiophene)-poly(styrene sulfonate)) with thickness ~ 30 nm was spin coated on cleaned substrate. In the subsequent step,

the photo-functional materials which is a blend of various ratios of doped CuO and P3HT was spin-coated over PEDOT-PSS at a speed of 1500 rpm for 20 s, and afterward at a rate of 500 rpm and 100 rpm/min for 20 s in order to remove the solvent completely. Finally, the top contact Al (80 nm) was deposited using thermal evaporator under high vacuum. All the devices with area (3×2 cm^2) were annealed at 90 °C for 15 min under argon flow to attain fine morphological distribution of the active blend.

SEM (HITACHI S-4800) and TEM (Tecnai F20 U-TWIN) were performed to examine the surface morphology of the prepared materials. EDX (HITACHI S-4800) was performed to investigate the elemental composition of the doped and un-doped samples. XRD (Rigaku D/MAXTTRIII) were recorded over a 2θ in the range from 20° to 80°. The absorption spectra of samples were collected by UV–Vis spectrophotometer (Shimadzu 1601) and the photoluminescence spectra of CuO and doped CuO nanotubes were recorded with a fluorescence spectrophotometer (Perkin Elmer LS 55) following excitation at 275 nm. The fabricated hybrid bulk hetero-junction solar cells were characterized by the current–voltage measurements, which were performed in air by using a tungsten halogen lamp (150 W) coupled with AM 1.5 G (Oriel 81086) filter and Keithley 2400 source meter. Lab View software was used to record the current–voltage measurements.

The structural and morphological characterization of Cu nanostructures were investigated by using SEM and TEM as shown in Fig. 1a–d respectively. These images represent that CuO exists in the form of nanotubes with an average diameter of 30–40 nm (Fig. 1a, c) whereas the doped CuO nanotubes have a slightly larger diameter of around 70–80 nm (Fig. 1b, d). In order to identify the presence of elements in the samples, EDX analysis was performed in the selected area of Cu-nanostructures (Fig. 2a, b). The observed peaks (Fig. 2a, b) for CuO index to the existence of copper, oxygen with atomic ratios 43.55% and 56.45% respectively. The spectrum of Mn:Fe:CuO represents the peak signals of Mn (0.84%) and Fe (0.59%) elements confirmed the successful incorporation in CuO nanotubes.

The crystal structures and phase information of CuO and doped CuO nanotubes were obtained by XRD (Fig. 3a). It is observed that the XRD pattern of synthesized samples shows high crystallinity upon doping with crystalline structures. The peak positions of CuO were observed to be at 110, − 111, 111, − 211, 020, 202, − 113, − 331, 220 and 331 planes well matched with JCPDS [00-005-0661]. It is noticeable that increasing doping concentration, the (− 111 and 111) peaks intensity was also increased considerably. Broadening of the diffraction peaks after doping depicts slightly crystallinity degeneration without the distortion in the crystal structure of CuO. The XRD results show that no peak was found related to Mn and Fe with impurity free phase which indicates that doping ions have substituted uniformly in the structure of host (CuO).

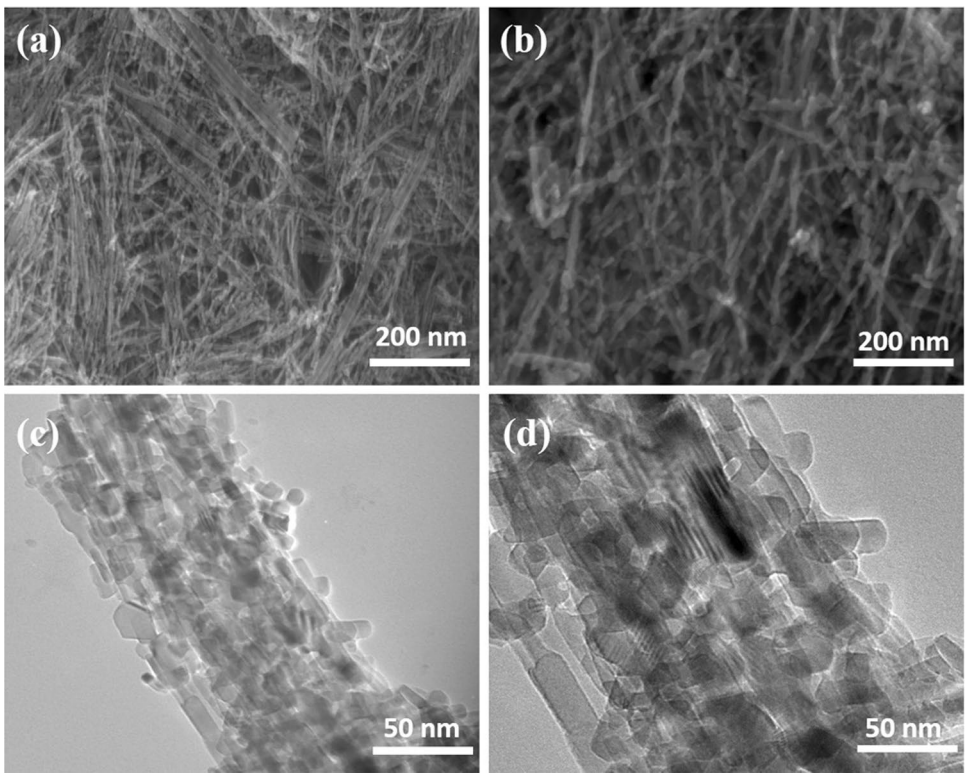

Fig. 1 **a**–**d** SEM and TEM studies of CuO nanotubes (**a**, **c**) and doped CuO nanotubes (**b**, **d**) respectively

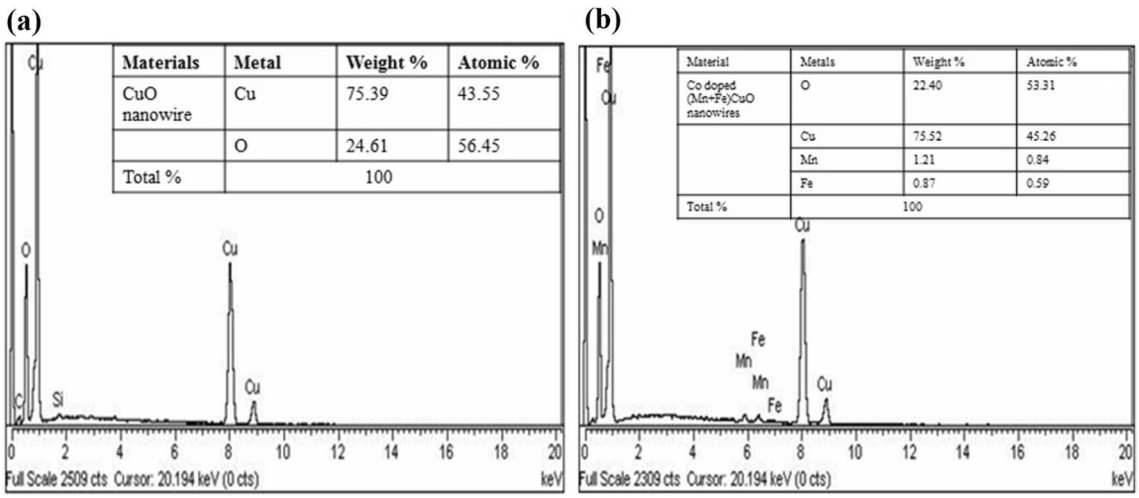

Fig. 2 **a**, **b** EDX Spectrum of CuO (**a**) and doped CuO nanotubes (**b**) respectively

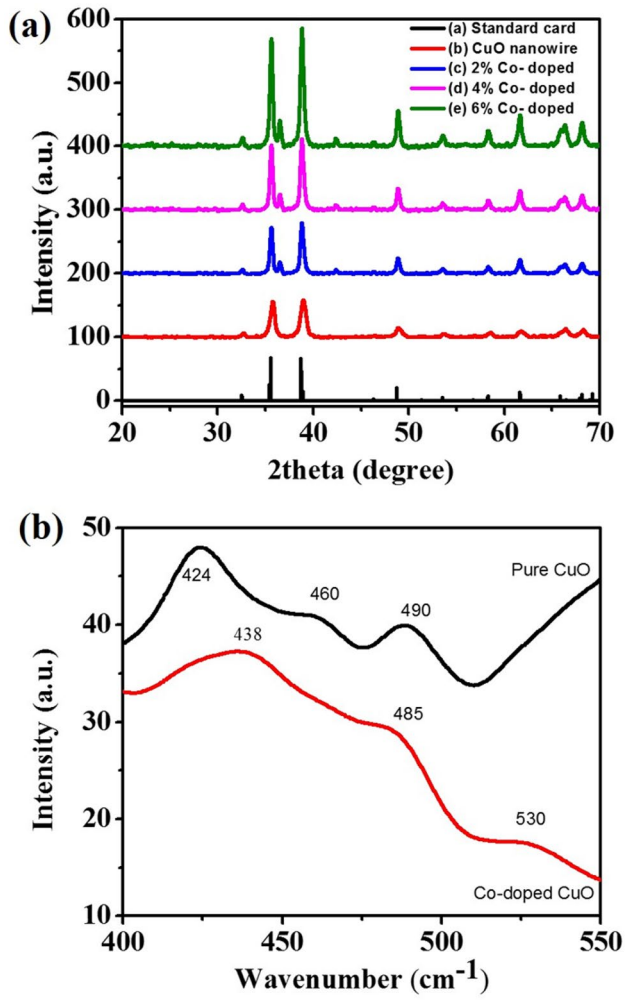

Fig. 3 **a**, **b** XRD pattern of samples (**a**) and emission spectra of pure and doped CuO nanotubes (**b**)

The emission spectra of control sample (CuO) have three main broad emission bands at 424, 460, and 490 nm are illustrated in Fig. 3b. The strong emission peaks at 424 and 438 nm are associated with the band-edge emission of CuO and Mn:Fe:CuO nanostructures respectively. The peaks positioned at (460 and 488) and (485 and 530) nm are caused by the band edge emission from the new sublevels at 273 K or due to the defects present in the CuO and doped CuO respectively [41–43]. The emission spectra of doped nanowires as compared to un-doped nanotubes shows strong red shift at 424 nm in control sample have shifted to 438 nm in doped CuO.

UV–visible absorption spectra of the synthesized doped CuO nanostructure with different ratios of (Mn and Fe) in DI water and band gap energies are shown in Fig. 4a, b. The absorption increased in the visible region upon mixing of Mn and Fe in CuO accompanied red shift. The observed red shift is attributed to the addition of Fe^{+3} and Mn^{+2} in CuO (Cu^{+2}). This addition has a major effect on the recombination time of charge carriers because doping ions introduce several new fermi levels above the valence band of CuO which further assist to absorb photons with less energy in the visible region. By enhancing the doping concentration, an increase in band gap was observed represent some defects with doping might cause intragap defect states [38]. The band gap energies calculated for CuO nanotubes is 1.98 eV, which is high than the reported for bulk CuO (1.85 eV) as shown in Fig. 4b [39]. This increase in the band gap of the nanotubes is credited to the well-known quantum confinement effect in semiconductors [40].

In order to calculate the band gap of CuO nanotubes, the Tauc Eq. (1) was used [39].

$$(\alpha h\nu)^n = B\left(h\nu - E_g\right) \quad (1)$$

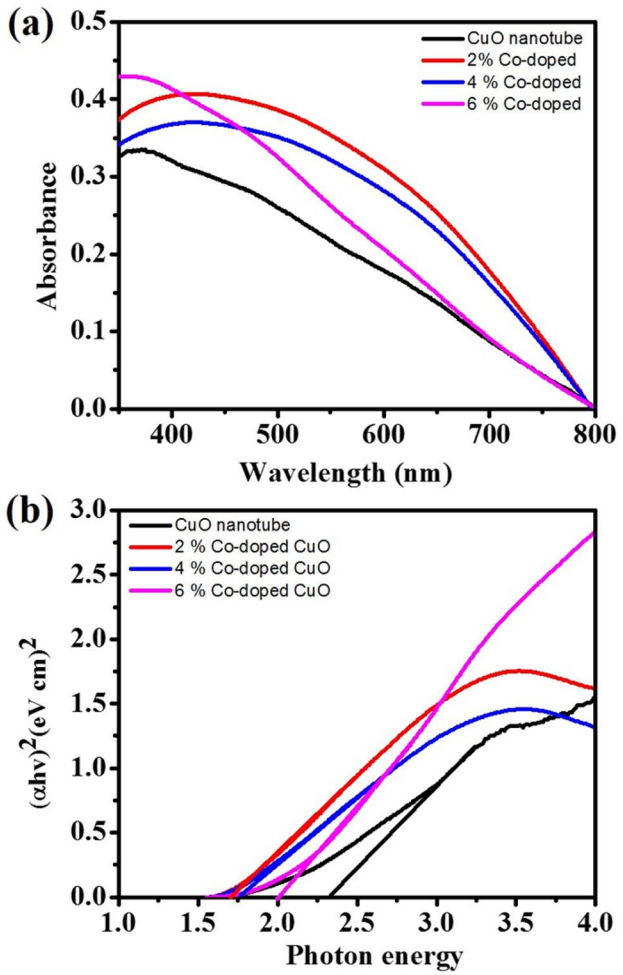

Fig. 4 **a**, **b** UV/Vis spectra of doped and undoped CuO (**a**) and band gap energies (**b**)

Here α is the absorption coefficient, hv is the photon energy, n = ½ for indirect transition and n = 2 for direct transition (semiconductor). The band gap of CuO and different percentage doped CuO were listed in Table 1.

Electrochemical impedance spectroscopy (EIS) is an effective technique to find out the interfacial properties of the materials in terms of the Nyquist plot. The Nyquist plot of doped and un-doped CuO nanotubes using 0.5 mM $[Fe(CN)6]^{3-/4-}$ as the redox probe were measured (Fig. 5). The plots for these electrodes material exhibited a typical semicircle and linear behavior in the high-frequency and low frequency regions respectively. The intercept of a real axis in the high-frequency region is the solution resistance. The diameter of the semicircle in plot denotes the charge-transfer resistance (R_{ct}), which reins the electron-transfer kinetics of the redox reaction at the electrode surface. This R_{ct} value feasible as a responsive parameter to describe the interfacial properties of electrode/electrolyte interface [43]. CuO nanotubes exhibited poor charge transfer kinetics as compared to doped samples (Fig. 5). The mixing of Mn and Fe (2%) in nanotubes exhibit lowest charge transfer resistance relative to other materials. Hence, the EIS results ensure the efficient charge separation achieved with the small amount of doping (2%) rather than higher amounts as well as CuO nanotubes.

Table 1 The band gap of CuO with different percentage of doped CuO

Material composition CuO:(Mn and Fe)%	λ_{max} (nm)	Bandgap (eV)
1:0	626	1.98
1:2	746	1.66
1:4	708	1.75
1:6	645	1.92

To examine the effect of doping on the photovoltaic performance, hybrid devices were fabricated with normal architecture (Fig. 6a). The primarily active layer is composed of electron donor P3HT and acceptor materials Mn:Fe (0, 2, 4 and 6)% doped CuO using methanol as a solvent. The energy level diagram of prepared hybrid BHJ organic devices is shown in Fig. 6b [25]. The photon energy was absorbed by photoactive materials (Fig. 6a, b), which generates excitons (e^- and h^+ pairs) at the D/A interface. The photogenerated electrons move toward lower C.B of the acceptor (CuO:Mn:Fe) to reach anode (Al) and holes transfer towards ITO after passing through thin hole transport film (PEDOT:PSS) (Fig. 6b). The J–V curves of fabricated devices were measured under dark and standard light conditions (100 mW cm^{-2}, AM 1.5) as shown in Fig. 6b. The obtained curves (Fig. 6c) show that power conversion efficiency-PCE improved with doping in CuO blended with P3HT compared to binary device (P3HT:CuO). The PCE increased from 0.50 to 0.84% with

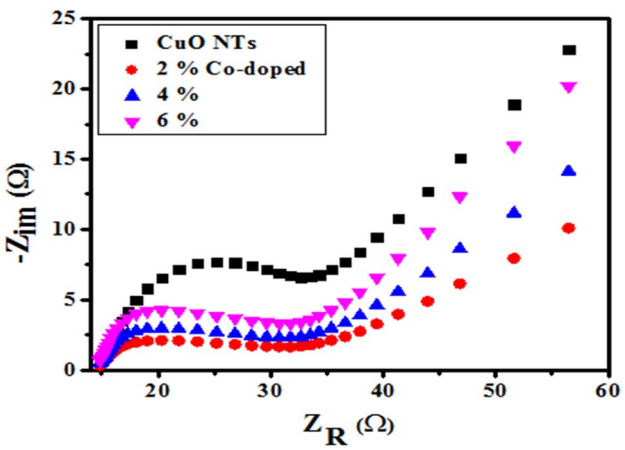

Fig. 5 Nyquist plot of the CuO and doped CuO nanotubes

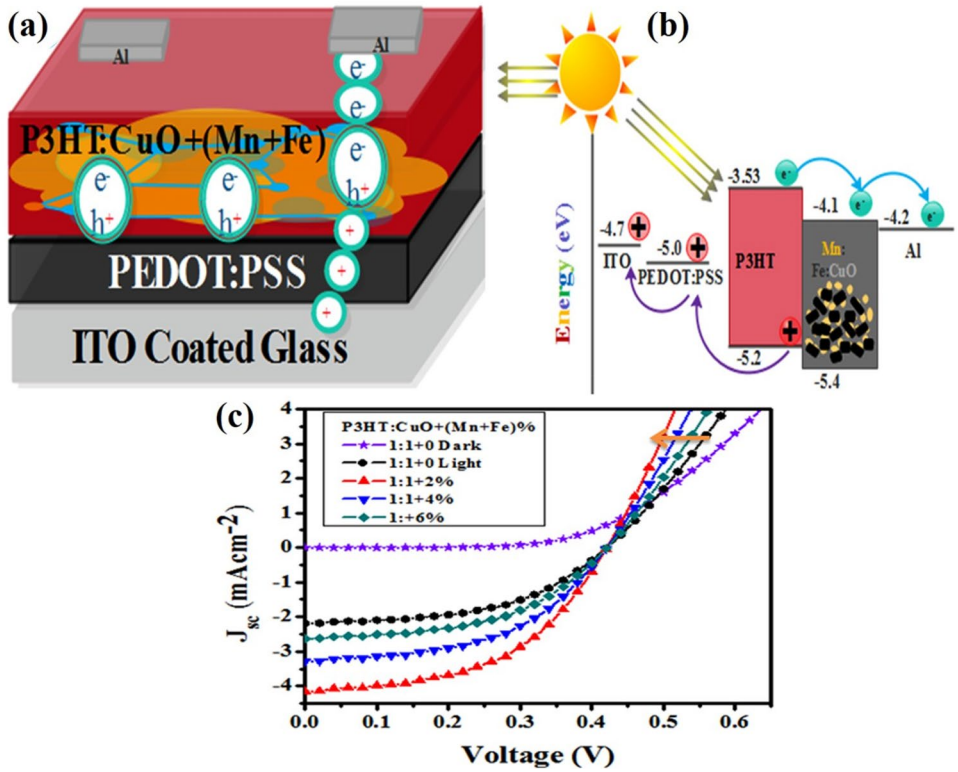

Fig. 6 **a** Schematic diagram of fabricated hybrid devices. **b** Energy level diagram. **c** J–V characteristics

Table 2 Electrical output parameters obtained from Fig. 6

Devices P3HT:CuO:(Mn + Fe)]%	Jsc (mA cm^2)	V_{oc} (V)	FF (%)	PCE (%)
1:1:0	2.18	0.41	0.49	0.50
1:1:0.02	4.1	0.40	0.52	0.84
1:1:0.04	3.2	0.40	0.51	0.66
1:1:0.06	2.6	0.41	0.50	0.54

an optimum amount (2%) of ions doped and this benefit decreased with high quantity of doping but still higher than the binary blended control device. The extracted electrical output parameters under illumination from the curves are shown in Table 2. We noticed, a significant increase in extracted parameters namely short-circuit current density and fill factor (FF) with ternary doping was found. This increase in efficiency is attributed to decrease in Rs-series resistance upon addition of Mn and Fe with CuO. The decrease in Rs is represented by a yellow arrow (Fig. 6c) upon mixing lead to increase in FF and hence PCE. The improvement in Jsc with optimized doping in CuO is associated to the high conductivity of nanotubes. But large amount of doping leads to the growth of oriented attachment to form nanotube surface rough, the creation of new defect and trapping states which trap the charge carriers caused to lower the Jsc [36, 38, 44].

In summary, Mn and Fe doped CuO nanostructures were synthesized via wet chemical method and characterized by XRD, EDX, SEM, TEM, spectroscopic techniques etc. The XRD studies reveal that both doped and un-doped CuO have single phase which suggesting the successfully doping of Mn and Fe in CuO lattice. As-synthesized materials were used in the hybrid bulk heterojunction organic solar cell and it was found that the low concentration of doping increase the charge separation led to enhance the power conversion efficiency of the device as compared to high amount of doping. This increase in the power conversion efficiency of the prepared devices is mostly due to increase in FF and Jsc upon doping of Mn:Fe to CuO nanostructures.

2 Summary statement

Recently, metal oxide nanomaterials with different architecture has been widely synthesized for various applications in electronics, optoelectronics, sensor, catalysis, solar cell etc. because of their unique electronic, optical, magnetic and morphological properties. Herein, transition metals i.e. Mn, Fe doped CuO nanostructures were synthesized via wet chemical method and characterized by X-ray diffractometer, scanning electron microscope, energy dispersive x-ray spectroscopy, transmission electron microscope, ultraviolet–visible and emission spectroscopy. The

XRD studies reveal that doped and un-doped CuO have single phase suggesting the incorporation of Mn and Fe dopants in CuO lattice. Further, as-synthesized materials were used in the hybrid bulk heterojunction organic solar cell and it was found that the low concentration of doping increase the charge separation led to enhance the power conversion efficiency of the device as compared to high amount of doping. This increase in the power conversion efficiency of the prepared devices is mostly due to increase in FF and Jsc upon doping of Mn:Fe to CuO nanostructures.

Acknowledgements This study is supported by Higher Education Commission (HEC), Pakistan and Mr. Iqbal also acknowledges the support from Chinese Academy of Science (CAS), China for research facilities.

Author contributions M. Iqbal and K. H. Thebo conceived and supervised the project; M. Iqbal and A. Ali designed the experiments; M. Iqbal performed the experiments with the help of A. Ali and analyzed the data. K. H. Thebo, M. Iqbal, A. Ali, S.K. Ahmad, R.F. Mehmood, J. Khan and K. Khan wrote and discuss the manuscript. All the authors discussed the results and commented on the manuscript.

Compliance with ethical standards

Competing interests The authors declare that they have no conflict of interest.

References

1. Ahmed S, Rasul M, Martens WN, Brown R, Hashib M (2010) Heterogeneous photocatalytic degradation of phenols in wastewater: a review on current status and developments. Desalination 261:3–18
2. Wang Z, Zhao S, Zhu S, Sun Y, Fang M (2011) Photocatalytic synthesis of M/Cu_2O (M = Ag, Au) heterogeneous nanocrystals and their photocatalytic properties. CrystEngComm 13:2262–2267
3. Sun S, Zhang X, Zhang J, Wang L, Song X, Yang Z (2013) Surfactant-free CuO mesocrystals with controllable dimensions: green ordered-aggregation-driven synthesis, formation mechanism and their photochemical performances. CrystEngComm 15:867–877
4. Shi W, Chopra N (2012) Controlled fabrication of photoactive copper oxide–cobalt oxide nanowire heterostructures for efficient phenol photodegradation. ACS Appl Mater Interfaces 4:5590–5607
5. Yang M, He J (2011) Fine tuning of the morphology of copper oxide nanostructures and their application in ambient degradation of methylene blue. J Colloid Interface Sci 355:15–22
6. Iqbal M, Ali A, Nahyoon NA, Majeed A, Pothu R, Phulpoto S, Thebo KH (2019) Photocatalytic degradation of organic pollutant with nanosized cadmium sulfide. Mater Sci Energy Technol 2:41–45
7. Pradeep U, Villani M, Calestani D, Cristofolini L, Iannotta S, Zappettini A, Coppedè N (2016) Charge-separation enhancement in inverted polymer solar cells by molecular-level triple heterojunction: NiO-np:P3HT:PCBM. Nanotechnology 28:035403
8. Chen P-Y, Yang S-H (2016) Improved efficiency of perovskite solar cells based on Ni-doped ZnO nanorod arrays and Li salt-doped P3HT layer for charge collection. Opt Mater Express 6:3651–3669
9. Colmenares J, Aramendia M, Marinas A, Marinas J, Urbano F (2006) Synthesis, characterization and photocatalytic activity of different metal-doped titania systems. Appl Catal A Gen 306:120–127
10. Almquist CB, Biswas P (2002) Role of synthesis method and particle size of nanostructured TiO_2 on its photoactivity. J Catal 212:145–156
11. Chen Y, Wang K, Lou L (2004) Photodegradation of dye pollutants on silica gel supported TiO_2 particles under visible light irradiation. J Photochem Photobiol A Chem 163:281–287
12. Kiriakidou F, Kondarides DI, Verykios XE (1999) The effect of operational parameters and TiO_2-doping on the photocatalytic degradation of azo-dyes. Catal Today 54:119–130
13. Akpan U, Hameed B (2009) Parameters affecting the photocatalytic degradation of dyes using TiO_2-based photocatalysts: a review. J Hazard Mater 170:520–529
14. Gao W, Yang S, Yang S, Lv L, Du Y (2010) Synthesis and magnetic properties of Mn doped CuO nanowires. Phys Lett A 375(2):180–182
15. Mariammal R, Ramachandran K, Kalaiselvan G, Arumugam S, Renganathan B, Sastikumar D (2013) Effect of magnetism on the ethanol sensitivity of undoped and Mn-doped CuO nanoflakes. Appl Surf Sci 270:545–552
16. Ravi S, Shashikanth FW (2015) Ferromagnetism in Mn doped copper oxide nanoflake like structures with high Neel temperature. Mater Lett 141:132–134
17. Sharma N, Gaur A, Kotnala R (2015) Signature of weak ferroelectricity and ferromagnetism in Mn doped CuO nanostructures. J Magn Magn Mater 377:183–189
18. Xu M, Yang L, Li Y, Guo Z, Zhang Y, Qiu H, Pan L (2011) Structural and magnetic properties of $Cu1-_xMn_xO$ nanocrystal prepared by combustion synthesis. Physica B Condens Matter 406(17):3180–3186
19. Choi W, Termin A, Hoffmann MR (1994) The role of metal ion dopants in quantum-sized TiO_2: correlation between photoreactivity and charge carrier recombination dynamics. J Phys Chem 98:13669–13679
20. Zhang Z, Wang C-C, Zakaria R, Ying JY (1998) Role of particle size in nanocrystalline TiO_2-based photocatalysts. J Phys Chem B 102:10871–10878
21. Ohtani B (2013) Titania photocatalysis beyond recombination: a critical review. Catalysts 3:942–953
22. Naidu BVK, Park JS, Kim SC, Park S-M, Lee E-J, Yoon K-J, Lee SJ, Lee JW, Gal Y-S, Jin S-H (2008) Novel hybrid polymer photovoltaics made by generating silver nanoparticles in polymer: fullerene bulk-heterojunction structures. Sol Energy Mater Sol Cells 92:397–401
23. Morfa AJ, Rowlen KL, Reilly TH III, Romero MJ, van de Lagemaat J (2008) Plasmon-enhanced solar energy conversion in organic bulk heterojunction photovoltaics. Appl Phys Lett 92:013504
24. Park M, Chin BD, Yu J-W, Chun M-S, Han S-H (2008) Enhanced photocurrent and efficiency of poly(3-hexylthiophene)/fullerene photovoltaic devices by the incorporation of gold nanoparticles. J Ind Eng Chem 14:382–386
25. Zoolfakar AS, Rani RA, Morfa AJ, Balendhran S, O'Mullane AP, Zhuiykov S, Kalantar-zadeh K (2012) Enhancing the current density of electrodeposited ZnO–Cu_2O solar cells by engineering their heterointerfaces. J Mater Chem 22:21767
26. Chen YC, Hsu CY, Lin RYY, Ho KC, Lin JT (2013) Materials for the active layer of organic photovoltaics: ternary solar cell approach. Chemsuschem 6:20–35
27. Honda S, Nogami T, Ohkita H, Benten H, Ito S (2009) Improvement of the light-harvesting efficiency in polymer/fullerene

bulk heterojunction solar cells by interfacial dye modification. ACS Appl Mater Interfaces 1:804–810
28. Xu H, Wada T, Ohkita H, Benten H, Ito S (2013) Dye sensitization of polymer/fullerene solar cells incorporating bulky phthalocyanines. Electrochim Acta 100:214–219
29. Yang L, Yan L, You W (2013) Organic solar cells beyond one pair of donor–acceptor: ternary blends and more. J Phys Chem Lett 4:1802–1810
30. Kalantar-zadeh K, Ou JZ, Daeneke T, Sasaki T, Fuhrer MS (2016) Two dimensional and layered transition metal oxides. Appl Mater Today 5:73
31. Zoolfakar AS, Rani RA, Morfa AJ, O'Mullane AP, Kalantar-zadeh K (2014) Nanostructured copper oxide semiconductors: a perspective on materials, synthesis methods and applications. J Mater Chem C 2:5247–5270
32. Oh SH, Heo SJ, Yang JS, Kim HJ (2013) Effects of ZnO nanoparticles on P3HT:PCBM organic solar cells with DMF-modulated PEDOT:PSS buffer layers. ACS Appl Mater Interfaces 5:11530–11534
33. Mittiga A, Salza E, Sarto F, Tucci M, Vasanthi R (2006) Heterojunction solar cell with 2% efficiency based on a Cu_2O substrate. Appl Phys Lett 88:163502
34. Herion J, Niekisch E, Scharl G (1980) Investigation of metal oxide/cuprous oxide heterojunction solar cells. Sol Energy Mater 4:101–112
35. Akimoto K, Ishizuka S, Yanagita M, Nawa Y, Paul GK, Sakurai T (2006) Thin film deposition of Cu_2O and application for solar cells. Sol Energy 80:715–722
36. Iqbal M, Sial MAZG, Shabbir S, Siddiq M, Iqbal A (2017) Effect of Fe doping on the crystallinity of CuO nanotubes and the efficiency of the hybrid solar cells. J Photochem Photobiol A Chem 335:112–118
37. Jiang T, Kong J, Wang Y, Meng D, Wang D, Yu M (2016) Optical and photocatalytic properties of Mn-doped CuO nanosheets prepared by hydrothermal method. Cryst Res Technol 51:58–64
38. Iqbal M, Thebo AA, Shah AH, Iqbal A, Thebo KH, Phulpoto S, Mohsin MA (2017) Influence of Mn-doping on the photocatalytic and solar cell efficiency of CuO nanowires. Inorg Chem Commun 76:71–76
39. Basith NM, Vijaya JJ, Kennedy LJ, Bououdina M (2013) Structural, optical and room-temperature ferromagnetic properties of Fe-doped CuO nanostructures. Physica E Low Dimens Syst Nanostruct 53:193–199
40. Ethiraj AS, Kang DJ (2012) Synthesis and characterization of CuO nanowires by a simple wet chemical method. Nanoscale Res Lett 7:70
41. Kliche G, Popovic Z (1990) Far-infrared spectroscopic investigations on CuO. Phys Rev B 42:10060
42. Zheng L, Liu X (2007) Solution-phase synthesis of CuO hierarchical nanosheets at near-neutral pH and near-room temperature. Mater Lett 61:2222–2226
43. Randviir EP, Banks CE (2013) Electrochemical impedance spectroscopy: an overview of bioanalytical applications. Anal Methods 5:1098–1115
44. Han J, Mantas P, Senos A (2002) Defect chemistry and electrical characteristics of undoped and Mn-doped ZnO. J Eur Ceram Soc 22:49–59